How to cite: *Angew. Chem. Int. Ed.* **2022,** *61,* e202115892
International Edition: doi.org/10.1002/anie.202115892
German Edition: doi.org/10.1002/ange.202115892

Spin Crossover

Spin Crossover in a Cobalt Complex on Ag(111)

Sven Johannsen, Sascha Ossinger, Jan Grunwald, Alexander Herman, Heiko Wende, Felix Tuczek, Manuel Gruber, and Richard Berndt**

Abstract: *The Co-based complex $[Co(H_2B(pz)(pypz))_2]$ (py = pyridine, pz = pyrazole) deposited on Ag(111) was investigated with scanning tunneling microscopy at ≈5 K. Due to a bis(tridentate) coordination sphere the molecules aggregate mainly into tetramers. Individual complexes in these tetramers undergo reversible transitions between two states with characteristic image contrasts when current is passed through them or one of their neighbors. Two molecules exhibit this bistability while the other two molecules are stable. The transition rates vary linearly with the tunneling current and exhibit an intriguing dependence on the bias voltage and its polarity. We interpret the states as being due to $S = {}^1/_2$ and ${}^3/_2$ spin states of the Co^{2+} complex. The image contrast and the orders-of-magnitude variations of the switching yields can be tentatively understood from the calculated orbital structures of the two spin states, thus providing first insights into the mechanism of electron-induced excited spin-state trapping (ELIESST).*

Introduction

Spin-crossover complexes may change their spin between a low-spin (LS) and a high-spin (HS) state depending on parameters such as temperature, light and current.[1–5] Employing different transition-metal ions (Fe, Co, Mn, Cr and Ni) and oxidation states[6–10] different spin states are accessible. Nonetheless, most investigations have so far dealt with Fe-based complexes. The LS to HS transition in Co complexes involves the transfer of a single electron from a t_{2g} to an e_g orbital, whereas two electrons are involved for Fe^{II} compounds. The corresponding change in the coordination bond lengths and molecular volume as well as the change in entropy upon spin crossover (SCO) are consequently smaller than for Fe complexes.[9] As a result, the thermal spin transition of Co SCO compounds is often more gradual because a smaller volume change leads to less cooperativity and it is more sensitive to the environment as small perturbations may easily overcome the entropy-driven SCO.

Investigations of SCO molecules in direct contact with metal surfaces, so far solely involving Fe-based compounds, have shown that the SCO properties usually deviate from those of the bulk material.[3,5,11–17] One may therefore speculate that Co complexes on metal surfaces may show similar SCO behavior as Fe molecules.

Although several examples of functional Fe-based SCO complexes in direct contact with surfaces have been reported,[12,17–33] the weakness of the coordination bonds has often been an issue.[14,29,34–36] Coordination bonding in Co complexes is expected to be even weaker owing to the larger population of the antibonding e_g orbitals. To increase the chance of success, we designed and synthesized a Co complex (Figure 1a) inspired by one of the most robust Fe^{2+} SCO compounds,[37] which is functional on Ag(111).[33] Here we show that the Co^{2+} compound, where spin states $S = {}^1/_2$ and $S = {}^3/_2$ are expected, aggregates into tetramers on Ag(111). The complexes are reversibly switched by the injection or extraction of electrons. Memristive characteristics are found although the molecules are directly adsorbed on a metal substrate without the intervening decoupling layer previously used for other compounds.[18,19,26,34] The data can be consistently understood in terms of SCO.

So far, little has been known about the mechanism leading to electron-induced excited spin-state trapping (ELIESST). The present case of $[Co(H_2B(pz)(pypz))_2]$ provides an opportunity to improve on this state of affairs. A distinct dependence of the switching yield on the current direction and spin state is observed and sets margins that a model of ELIESST has to respect. Below we outline a model that fulfills this requirement.

Results and Discussion

$[Co(H_2B(pz)(pypz))_2]$ is a complex with linear tridentate ligands (Figures 1a–c).[33,37] The integrity of the molecules upon sublimation has been verified with complementary

[*] S. Johannsen, M. Gruber, R. Berndt
Institut für Experimentelle und Angewandte Physik, Christian-Albrechts-Universität, 24098 Kiel (Germany)
E-mail: manuel.gruber@uni-due.de
berndt@physik.uni-kiel.de
S. Ossinger, J. Grunwald, F. Tuczek
Institut für Anorganische Chemie, Christian-Albrechts-Universität, 24098 Kiel (Germany)
S. Ossinger
Department of Chemistry, University of Basel, St. Johanns-Ring 19, 4056 Basel (Switzerland)
A. Herman, H. Wende, M. Gruber
Faculty of Physics and CENIDE, University of Duisburg-Essen, 47057 Duisburg (Germany)

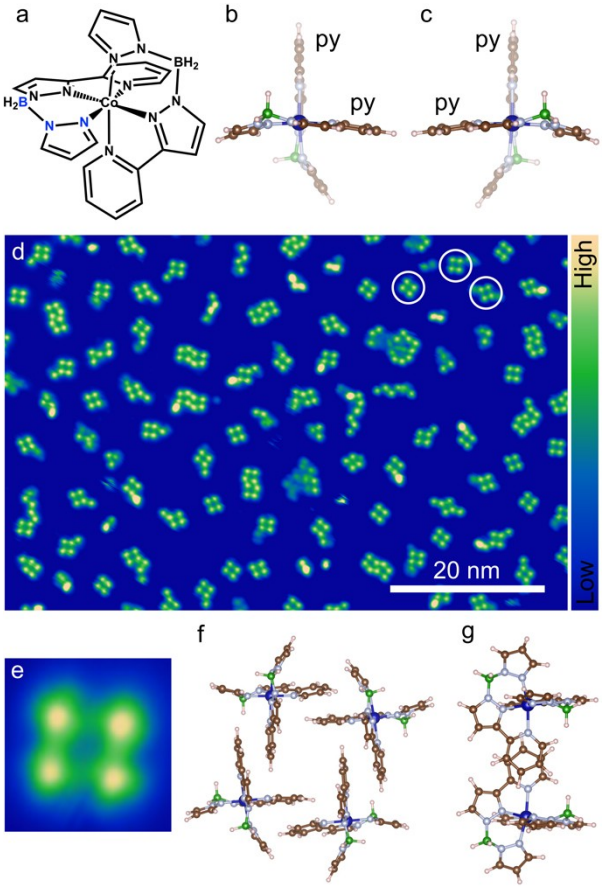

Figure 1. a) Structure of $[Co(H_2B(pz)(pypz))_2]$. b) and c) Suggested geometries of the two enantiomers of adsorbed complexes viewed from the vacuum side. The atoms of the lower ligand are semi-transparent. Blue: Co, gray: N, brown: C, rose: H, green: B. d) Constant-current topograph (sample voltage −0.5 V, current 10 pA, 72×48 nm^2). The main structural motifs are tetramers although some smaller structures and touching tetramers are observed, too. Examples of the three observed cluster orientations are indicated by circles. The false colors cover a height range of 300 pm. e) Detailed topograph of a rectangular tetramer (3.15 nm wide). Each complex gives rise to a featureless protrusion. f) Model of the tetramer shown in (e). Two identical enantiomers are arranged on each of the diagonals of the rectangle. g) View from the right side of the model in (f). The substrate (not shown) would be on the right. Only two complexes are included for clarity.

X-ray photoelectron spectroscopy and infrared spectroscopy measurements (Supporting Information). Figure 1d displays an overview of Ag(111) with sub-monolayer coverage. The complexes aggregate into rectangular tetramers although a degree of disorder is present. A detailed image of a tetramer (Figure 1e) reveals separations between topographic maxima of ≈1 and ≈1.15 nm, which are virtually identical to those observed of $[Fe(H_2B(pz)(pypz))_2]$ tetramers.[33] Even the apparent heights, which are fairly bias-independent in the range $|V|<1$ V, are similar to the Fe case. The proposed structure of the tetramers is consequently the same as previously determined for the Fe compound (Figure 1f). The tetramers involve both enantiomers of $[Co(H_2B(pz)(pypz))_2]$ (Figures 1b and c) and are stabilized by π–π interactions.

Stable imaging of the tetramers is possible as long as $|V| \lesssim 1$ V. Beyond this range, the current jumps between two levels when the tip is placed above either of two of the molecules of each cluster. The current-voltage characteristic (Figure 2a) displays two distinct evolutions marked L and H that may repeatedly be measured. Transitions between the levels occur at $|V| \gtrsim 1$ V and appear as vertical line segments in the graph. When the voltage is reduced below the range where switching occurs, the state of the molecule is frozen and can be imaged. Figures 2b and c display a typical pair of images. In the pristine cluster (Figure 2b), all molecules are in the L state.

Decreasing the negative voltage (and the current, owing to open-feedback conditions) to −1 V on the molecule indicated by L causes a change to H. The apparent height slightly increases and the topograph displays clear intramolecular structure.

Transitions can also be induced in the molecule on the other end of the diagonal when the tip is moved above that molecule. The other two molecules, however, remain stable, even at more harsh conditions. This striking effect was previously observed from $[Fe(H_2B(pz)(pypz))_2]$ tetramers and attributed to their geometrical structure.[33] The terminal-pyrazole moieties, which display the largest geometrical change during the Fe spin transition from $S=0$ to $S=2$, are sterically blocked for two molecules while the other two pz are free to move. Similar to the case of $[Fe(H_2B(pz)(pypz))_2]$ tetramers, injecting current into the stable molecules induces switching of their closest neighbors.[33]

Figures 3 a and d present time series of the current for negative and positive sample voltages. The data were recorded after placing the tip above a switchable molecule. Clear two-level fluctuations are observed. At both polarities, the magnitude of the current predominantly is low and short

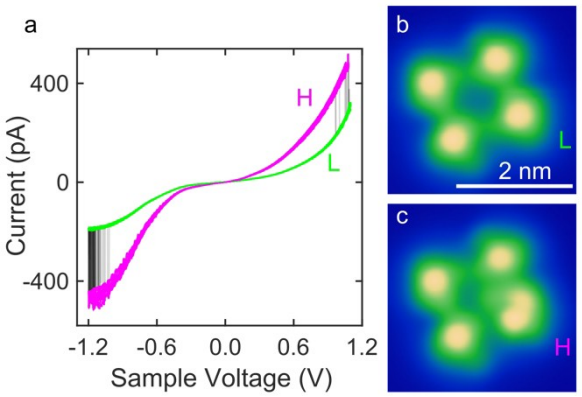

Figure 2. a) Current–voltage data recorded from a molecule in a tetramer. 16 sweeps of the sample voltage between −1.2 to 1.1 V and back are shown. Abrupt transitions between two states denoted L and H are observed at $|V|>1$ V, and lead to hysteresis. b) Image of a tetramer in its pristine state. c) Image recorded after current injection ($V=-1$ V, $I=-18$ pA, duration 1 s) to the molecule marked with an L in (b). In its new state H, the molecule displays intramolecular contrast. Images recorded at −0.5 V and 10 pA.

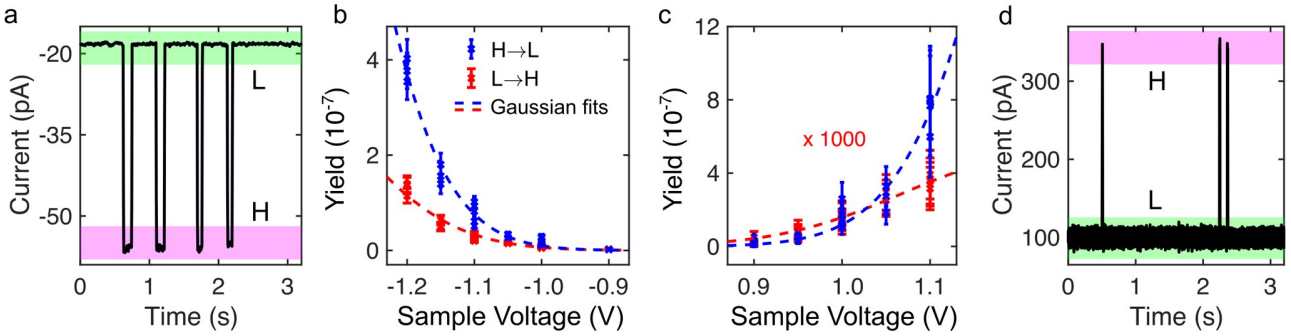

Figure 3. a) Time series of the tunneling current through a switchable molecule in a tetramer at negative sample bias $V=-1$ V with open feedback loop. From its initial level denoted L the current approximately doubles to level H. Changes occur abruptly with a rate of $\approx$1/s. b) Switching yield, i.e. the number of switching events per tunneling electron, at negative voltages for transitions from H to L (blue) and vice versa (red). Dashed lines indicate Gaussian fits to the data. The yields were determined from measurements with durations between 20 and 180 s and 42 to 177 switching events (procedure outlined in the Supporting Information to ref. [33]). The error margins indicate one standard deviation assuming Poisson statistics. c) Yields at positive sample voltage. d) Time series at $V=1$ V. The molecule is predominantly in its L state with short intermissions of H. The time series have been acquired for different tip-sample distances to obtain rates that can be conveniently measured.

excursions to high values occur over sub-second intervals. From these and similar data, we determined transition rates as functions of the sample voltage. The rates are proportional to the current (Supporting Information, Figure S1) suggesting that the transitions are caused by one-electron processes and motivating the definition of a switching yield as the probability of an electron to induce a transition.

Figures 3b and c display yield data. At both bias polarities, we observe non-zero yields when $|V|$ exceeds 0.9 V. The corresponding electron energies are much larger than vibrational energies of the metal-organic compounds. In particular, the N–Co–N stretch modes relevant for the spin crossover transition are calculated to lie below 150 meV. It does therefore not appear likely that the transitions are caused by vibrational excitation alone.

We suggest that the observed current-induced transitions are spin transitions between the $S=1/2$ and $S=3/2$ states of the Co ion. Several indications render this interpretation most likely. First, we prepared the closed-shell complex $[Zn(H_2B(pz)(pypz))_2]$ on the same Ag(111) substrate and found tetramers which are almost indistinguishable from the Co compound.[33] Despite this similarity, however, the Zn complex does not exhibit the transitions observed in the Co case. This directly indicates the relevance of the partly filled *d*-shell of Co. Second, the similarities with the SCO compound $[Fe(H_2B(pz)(pypz))_2]$ are striking. Tetramers of both compounds exhibit transitions only in two molecules that are located opposite to each other on a diagonal. This effect can be understood from the structure of the tetramers in combination with the geometrical change that accompanies the spin transition.[33] The angle between the terminal pyrazole subunit and the pypz plane of the $H_2B(pz)(pypz)$ ligand it belongs to is significantly larger in the high spin state of both Fe and Co. The required free space is not available for two of the constituents of the tetramers, which prevents them from switching.

Finally, the difference of the topographic images of the two states is remarkable. While the pristine L state is imaged as a fairly featureless protrusion, images of the H state exhibit a nodal line that approximately points to the center of the tetramer. As discussed below, this feature is consistent with differences between the electronic structures of the LS and HS states. Unfortunately, a detailed and reliable image calculation of the clusters is not within reach. We therefore considered the orbitals obtained from our gas-phase DFT calculations. In contrast to the case of Fe-based compounds,[18,33] where the spin transition is accompanied by a substantial change of the gap between the highest occupied and the lowest unoccupied molecular orbitals (HOMO, LUMO), the orbital energies of $[Co(H_2B(pz)(pypz))_2]$ change less and do not directly lead to an image interpretation. However, an inspection of the spin-state dependence of the frontier orbitals suggests the following scenario.

Several of the orbitals exhibit significant density above the upper half of the molecule, in particular above the central pyrazole moiety, and thus presumably contribute to the tunneling current. However, upon the spin transition, one particular orbital, the LUMO, shows a drastic change that matches the image change. For illustration, we use a molecule from the lower left corner of a tetramer in its low- and high-spin states (Figure 4a and b). Our calculations predict essentially identical lowest unoccupied orbitals for α and β spins in the low-spin state (Figures 4c and e). The HS, α channel (Figure 4d) is also very similar, except for some geometrical distortion. However, the lowest unoccupied orbital of β spin in the HS state—the LUMO—looks strikingly different and exhibits a high density at the terminal pyrazole moiety, where the other unoccupied orbitals have little weight (Figure 4f). This orbital has a nodal plane along the pyrazole that approximately matches the orientation of the nodal line in the experimental image. A side view of the orbital (not shown) reveals that this part of the LUMO is located particularly high above the substrate. Moreover, it is much closer to the Fermi level than any other unoccupied orbital and it extends throughout the molecule. Both factors make it a likely candidate for high conductance. Finally, the composite image comprising a scaled model of the tetramer and its STM image (Figure 4g)

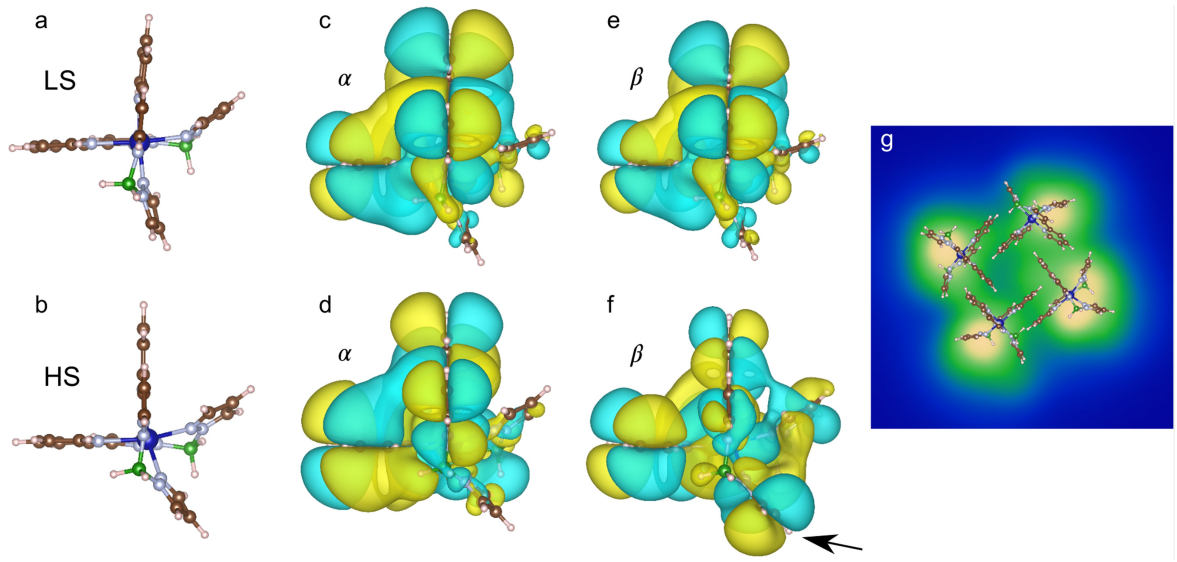

Figure 4. a), b) Optimized models of the LS and HS states of a gas-phase $[Co(H_2B(pz)(pypz))_2]$ molecule. Calculated spin α and spin β lowest unoccupied molecular orbitals for c), e) the LS, $S=^1/_2$ state, and d), f) HS, $S=^3/_2$ state. An arrow indicates the high density of states at the terminal pz subunit in the β channel. g) Superposition of a model cluster on the STM image of a tetramer. Only the molecule in the lower righthand corner is in the $S=^3/_2$ state.

reveals that the lateral position of this key orbital and the image contrast are fairly consistent.

Unfortunately, the spectroscopic data do not exhibit the fingerprints of spin excitations or a Kondo effect, which could help to more directly identify the spin states involved. Acquisition of spectroscopy data to identify orbitals was unsuccessful as well because of the high switching rates and diffusion occurring at larger voltages, even with small currents in the pA range. We therefore rely on the image contrast and consequently favor $S=^1/_2$ as being the pristine states of the complex on Ag(111). While $[Co(H_2B(pz)(pypz))_2]$ has a $S=^3/_2$ ground state in bulk material,[37] several studies have shown that the interaction with a metal substrate and possibly with neighbors can—even in the case of Fe compounds—lead to, e.g., the coexistence of both states.[12,14,19,22,24,38,39] Moreover, cobalt complexes with similar structural and electronic properties have been found to exhibit or lack thermal SCO in the bulk, indicating the importance of intermolecular interactions.[40–42]

The SCO properties are not expected to significantly vary with temperature. First, no thermal spin transition is observed in a 3 ML-thick film of the Co complex on Ag(111) as revealed by x-ray photoemission data acquired at 100 and 300 K (Supporting Information). Second, thermal energy is negligible relative to that of the tunneling electrons inducing switching (on the order of an electronvolt). Higher temperatures would most probably increase the mobility of the molecules on the surfaces and significantly complicate STM measurements.

Next, we discuss the yield data of Figure 3. Intriguingly, the yield of the L to H transition at positive sample bias is three orders of magnitude lower than the other measured yields, which in turn are fairly similar to each other. Below, we discuss a tentative model to describe ELIESST by considering electron/hole injection into the d-orbitals of the Co^{II} complex and a ligand-type orbital, L*. This model predicts a negligible yield of the L to H transition at positive sample voltage, in agreement with the experimental results.

The symmetry of the ligand field around the Co atom is not perfectly octahedral but rather exhibits a tetragonal distortion, which lifts the degeneracy of the t_{2g} and e_g orbitals. In the HS state, both d_{z^2} and $d_{x^2-y^2}$ orbitals along with the three t_{2g} orbitals at lower energy are occupied with α-spin electrons whereas two of the t_{2g} orbitals are occupied with β-spin electrons (Supporting Information, Figure S3). In the LS state, the three t_{2g} orbitals d_{xy}, d_{xz} and d_{yz} are doubly occupied and one additional α-spin electron occupies $d_{x^2-y^2}$ while the other e_g-orbital, d_{z^2}, is empty (Figure S4). In fact, the situation is slightly more involved in the title complex because the molecular z-axis re-orientates in the LS state. However, as shown in the Supporting Information, this leaves the essence of the proposed model of electron-induced spin-state switching unaffected. For simplicity, we therefore neglect this change of coordinate system. The calculations indicate that the lowest unoccupied orbitals of the complex have ligand character. We refer to them as L*.

For a positive sample voltage $V>0$, an electron is first transferred from the tip into L*, and the additional negative charge on the molecule is removed by transfer of an electron from one of the highest-energy occupied orbitals (i.e., a d-orbital) to the substrate. The individual molecules in the tetramer are oriented with their axes connecting the two central pyrazole moieties perpendicular to the surface, in the direction of the tip. Denoting these axes as z, electron transfer from the molecule to the substrate will predominantly be mediated by d_{z^2} and, to a lesser extent, by d_{xz} and d_{yz} orbitals whereas no or little electron transfer will proceed via orbitals in the corresponding xy-plane; i.e., $d_{x^2-y^2}$ and d_{xy}.

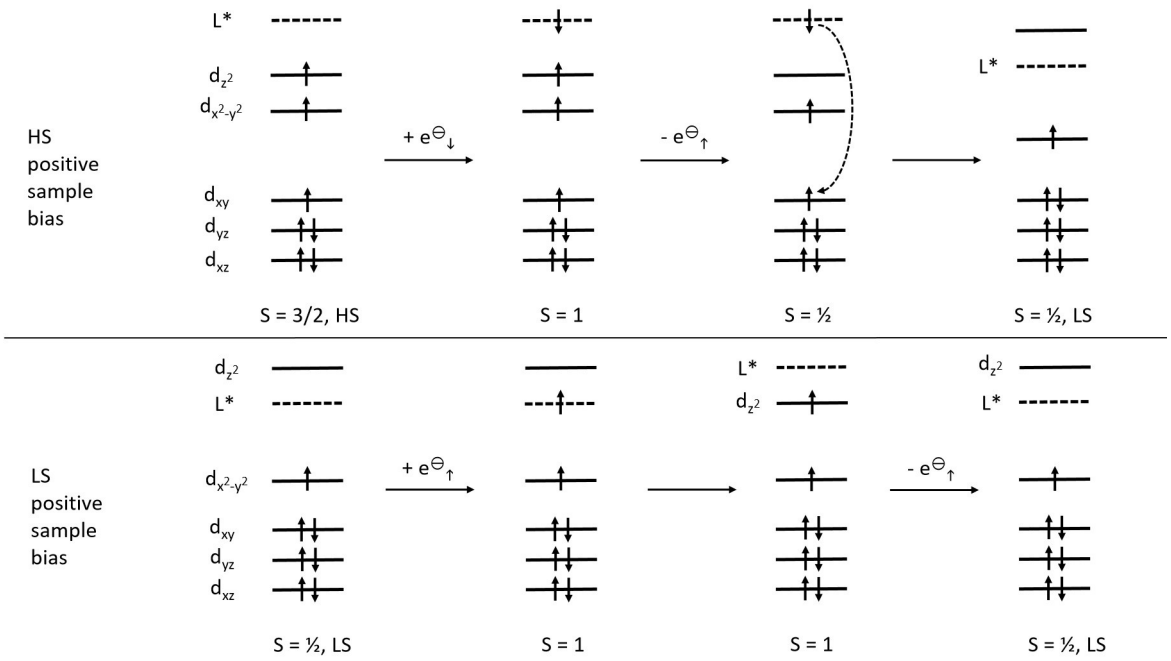

Figure 5. Schematic diagrams of the transitions from HS to LS (upper panel) and vice versa (lower panel) at positive sample voltage. Up and down arrows represent α- and β-spin electrons, respectively.

At negative sample voltage, an electron is first transferred from an occupied d-orbital to the tip, following the same rules, and the hole on the molecule is filled by transfer of an electron from the substrate to the L* orbital of the cationic complex (Supporting Information, Figure S2).

If the incoming and the outgoing electrons in the described electron-in/electron-out processes carry different spins, spin-state switching ensues. Taking the highspin ($S=$ $^3/_2$) state of Co^{II} at $V>0$ as an example (Figure 5, top), a β-spin electron is first transferred to L*. This generates an anionic (Co^{I}) $S=1$ state which subsequently releases an electron to the substrate. Among the occupied d-orbitals of Co^{I}, the best coupling is provided by d_{z^2} (see above) whence the electron is removed from it with the highest probability. If it carries a β spin, an excited $S=^1/_2$ state of Co^{II} results which rapidly relaxes to the LS ground state, completing the spin state switching process.

As detailed in the Supporting Information, Figure S2, similar scenarios can be conceived to account for HS→LS and LS→HS switching at negative sample voltages. However, an analogous mechanism is much less probable for LS→HS transitions at $V>0$ (Figure 5, lower panel). In order to induce switching to $S=^3/_2$, the spin has first to increase to $S=1$. This occurs through transfer of an α electron from the tip to L* which is at lower energy than d_{z^2}. However, electronic relaxation of the resulting Co^{I} state leads to a configuration in which the additional electron occupies d_{z^2}. As this orbital efficiently couples to the substrate the electron is rapidly removed from the molecule, restoring the original spin state. In the unlikely event that an electron is removed from the d_{xz} and d_{yz} orbitals despite the d_{z^2} state being occupied, $S=^3/_2$ may be obtained. In summary, this scenario is consistent with the experimental observation of a low LS→HS switching rate at $V>0$.

Conclusion

The present results illustrate that molecules assembled into nanoscale structures can exhibit unusual spin crossover phenomena. In the present case, electron induced spin state trapping (ELIESST) is observed from a tridentate Co compound that is robust enough to enable detailed measurements of switching yields and image contrasts. We propose a first tentative model of ELIESST that takes into account the orbital structure of the compound and qualitatively explains yield data. The results further indicate that molecular interactions drastically affect the switching capability of individual molecules. However, no decoupling layer is required to preserve the memristive functionality of the molecules directly on a metal substrate.

Acknowledgements

We thank Troels Markussen for preliminary calculations and discussions. Financial support from the European Union's Horizon 2020 program, Grant No. 766726 is acknowledged. H.W. and A.H. acknowledge financially support by the Deutsche Forschungsgemeinschaft (DFG, German Research Foundation) through the Collaborative Research Centre (CRC) 1242 (Project No. 278162697) and

project WE 2623/17-1 No. 389895192. Open Access funding enabled and organized by Projekt DEAL.

Conflict of Interest

The authors declare no conflict of interest.

Data Availability Statement

The data that support the findings of this study are available from the corresponding author upon reasonable request.

Keywords: Electron Transfer · Molecular Devices · Scanning Probe Microscopy · Single-Molecule Studies · Spin Crossover

[1] P. Gütlich, H. A. Goodwin, *Topics in Current Chemistry, Vol. 234*, Springer Heidelberg, Berlin, **2004**, pp. 1–47.
[2] G. Molnár, L. Salmon, W. Nicolazzi, F. Terki, A. Bousseksou, *J. Mater. Chem. C* **2014**, *2*, 1360.
[3] M. Gruber, R. Berndt, *Magnetochemistry* **2020**, *6*, 35.
[4] K. S. Kumar, M. Ruben, *Angew. Chem. Int. Ed.* **2021**, *60*, 7502–7521; *Angew. Chem.* **2021**, *133*, 7578–7598.
[5] L. Kipgen, M. Bernien, F. Tuczek, W. Kuch, *Adv. Mater.* **2021**, *33*, 2008141.
[6] P. E. Figgins, D. H. Busch, *J. Am. Chem. Soc.* **1960**, *82*, 820–824.
[7] D. Reinen, C. Friebel, V. Propach, *Z. Anorg. Allg. Chem.* **1974**, *408*, 187–204.
[8] Y. Garcia, P. Gütlich, *Spin Crossover in Transition Metal Compounds II, Vol. 234*, Springer Heidelberg, Berlin, **2004**, pp. 49–62.
[9] H. A. Goodwin, *Spin Crossover in Transition Metal Compounds II, Vol. 234*, Springer Heidelberg, Berlin, **2004**, pp. 23–47.
[10] S. Hayami, Y. Komatsu, T. Shimizu, H. Kamihata, Y. H. Lee, *Coord. Chem. Rev.* **2011**, *255*, 1981–1990.
[11] M. Gruber, V. Davesne, M. Bowen, S. Boukari, E. Beaurepaire, W. Wulfhekel, T. Miyamachi, *Phys. Rev. B* **2014**, *89*, 195415.
[12] M. Gruber, T. Miyamachi, V. Davesne, M. Bowen, S. Boukari, W. Wulfhekel, M. Alouani, E. Beaurepaire, *J. Chem. Phys.* **2017**, *146*, 092312.
[13] T. Jasper-Tönnies, M. Gruber, S. Karan, H. Jacob, F. Tuczek, R. Berndt, *J. Phys. Chem. Lett.* **2017**, *8*, 1569–1573.
[14] S. Ossinger, H. Naggert, L. Kipgen, T. JasperToennies, A. Rai, J. Rudnik, F. Nickel, L. M. Arruda, M. Bernien, W. Kuch, R. Berndt, F. Tuczek, *J. Phys. Chem. C* **2017**, *121*, 1210–1219.
[15] K. S. Kumar, M. Studniarek, B. Heinrich, J. Arabski, G. Schmerber, M. Bowen, S. Boukari, E. Beaurepaire, J. Dreiser, M. Ruben, *Adv. Mater.* **2018**, *30*, 1705416.
[16] L. Zhang, Y. Tong, M. Kelai, A. Bellec, J. Lagoute, C. Chacon, Y. Girard, S. Rousset, M. Boillot, E. Rivière, T. Mallah, E. Otero, M. Arrio, P. Sainctavit, V. Repain, *Angew. Chem. Int. Ed.* **2020**, *59*, 13341–13346; *Angew. Chem.* **2020**, *132*, 13443–13448.
[17] S. Ossinger, L. Kipgen, H. Naggert, M. Bernien, A. J. Britton, F. Nickel, L. M. Arruda, I. Kumberg, T. A. Engesser, E. Golias, C. Näther, F. Tuczek, W. Kuch, *J. Phys. Condens. Matter* **2020**, *32*, 114003.
[18] T. G. Gopakumar, F. Matino, H. Naggert, A. Bannwarth, F. Tuczek, R. Berndt, *Angew. Chem. Int. Ed.* **2012**, *51*, 6262–6266; *Angew. Chem.* **2012**, *124*, 6367–6371.
[19] T. Miyamachi, M. Gruber, V. Davesne, M. Bowen, S. Boukari, L. Joly, F. Scheurer, G. Rogez, T. K. Yamada, P. Ohresser, E. Beaurepaire, W. Wulfhekel, *Nat. Commun.* **2012**, *3*, 938.
[20] M. Bernien, D. Wiedemann, C. F. Hermanns, A. Krüger, D. Rolf, W. Kroener, P. Müller, A. Grohmann, W. Kuch, *J. Phys. Chem. Lett.* **2012**, *3*, 3431–3434.
[21] T. Palamarciuc, J. C. Oberg, F. El Hallak, C. F. Hirjibehedin, M. Serri, S. Heutz, J. F. Létard, P. Rosa, *J. Mater. Chem.* **2012**, *22*, 9690–9695.
[22] B. Warner, J. C. Oberg, T. G. Gill, F. El Hallak, C. F. Hirjibehedin, M. Serri, S. Heutz, M. A. Arrio, P. Sainctavit, M. Mannini, G. Poneti, R. Sessoli, P. Rosa, *J. Phys. Chem. Lett.* **2013**, *4*, 1546–1552.
[23] M. Bernien, H. Naggert, L. M. Arruda, L. Kipgen, F. Nickel, J. Miguel, C. F. Hermanns, A. Krüger, D. Krüger, E. Schierle, E. Weschke, F. Tuczek, W. Kuch, *ACS Nano* **2015**, *9*, 8960–8966.
[24] K. Bairagi, O. Iasco, A. Bellec, A. Kartsev, D. Li, J. Lagoute, C. Chacon, Y. Girard, S. Rousset, F. Miserque, Y. J. Dappe, A. Smogunov, C. Barreteau, M.-L. Boillot, T. Mallah, V. Repain, *Nat. Commun.* **2016**, *7*, 12212.
[25] W. Kuch, M. Bernien, *J. Phys. Condens. Matter* **2017**, *29*, 023001.
[26] T. Jasper-Toennies, M. Gruber, S. Karan, H. Jacob, F. Tuczek, R. Berndt, *Nano Lett.* **2017**, *17*, 6613.
[27] L. Kipgen, M. Bernien, F. Nickel, H. Naggert, A. J. Britton, L. M. Arruda, E. Schierle, E. Weschke, F. Tuczek, W. Kuch, *J. Phys. Condens. Matter* **2017**, *29*, 394003.
[28] L. Kipgen, M. Bernien, S. Ossinger, F. Nickel, A. J. Britton, L. M. Arruda, H. Naggert, C. Luo, C. Lotze, H. Ryll, F. Radu, E. Schierle, E. Weschke, F. Tuczek, W. Kuch, *Nat. Commun.* **2018**, *9*, 2984.
[29] S. Rohlf, J. Grunwald, T. Jasper-Toennies, S. Johannsen, F. Diekmann, M. Studniarek, R. Berndt, F. Tuczek, K. Rossnagel, M. Gruber, *J. Phys. Chem. C* **2019**, *123*, 17774.
[30] T. Brandl, S. Johannsen, D. Häussinger, N. Suryadevara, A. Prescimone, S. Bernhard, M. Gruber, M. Ruben, R. Berndt, M. Mayor, *Angew. Chem. Int. Ed.* **2020**, *59*, 15947; *Angew. Chem.* **2020**, *132*, 16081.
[31] S. Rohlf, J. Grunwald, M. Kalläne, J. Kähler, F. Diekmann, S. Ossinger, B. Flöser, F. Tuczek, K. Rossnagel, M. Gruber, *J. Phys. Chem. C* **2021**, *125*, 14105–14116.
[32] S. Thakur, E. Golias, I. Kumberg, K. Senthil Kumar, R. Hosseinifar, J. Torres-Rodríguez, L. Kipgen, C. Lotze, L. M. Arruda, C. Luo, F. Radu, M. Ruben, W. Kuch, *J. Phys. Chem. C* **2021**, *125*, 13925–13932.
[33] S. Johannsen, S. Ossinger, T. Markussen, F. Tuczek, M. Gruber, R. Berndt, *ACS Nano* **2021**, *15*, 11770–11778.
[34] T. G. Gopakumar, M. Bernien, H. Naggert, F. Matino, C. F. Hermanns, A. Bannwarth, S. Mühlenberend, A. Krüger, D. Krüger, F. Nickel, W. Walter, R. Berndt, W. Kuch, F. Tuczek, *Chem. Eur. J.* **2013**, *19*, 15702–15709.
[35] S. Gueddida, M. Gruber, T. Miyamachi, E. Beaurepaire, W. Wulfhekel, M. Alouani, *J. Phys. Chem. Lett.* **2016**, *7*, 900–904.
[36] T. Knaak, C. González, Y. J. Dappe, G. D. Harzmann, T. Brandl, M. Mayor, R. Berndt, M. Gruber, *J. Phys. Chem. C* **2019**, *123*, 4178–4185.
[37] S. Ossinger, C. Näther, A. Buchholz, M. Schmidtmann, S. Mangelsen, R. Beckhaus, W. Plass, F. Tuczek, *Inorg. Chem.* **2020**, *59*, 7966–7979.
[38] A. Pronschinske, R. C. Bruce, G. Lewis, Y. Chen, A. Calzolari, M. Buongiorno-Nardelli, D. A. Shultz, W. You, D. B. Dougherty, *Chem. Commun.* **2013**, *49*, 10446–10452.
[39] C. Fourmental, S. Mondal, R. Banerjee, A. Bellec, Y. Garreau, A. Coati, C. Chacon, Y. Girard, J. Lagoute, S. Rousset, M. L.

Boillot, T. Mallah, C. Enachescu, C. Barreteau, Y. J. Dappe, A. Smogunov, S. Narasimhan, V. Repain, *J. Phys. Chem. Lett.* **2019**, *10*, 4103–4109.
[40] M. G. Cowan, J. Olguín, S. Narayanaswamy, J. L. Tallon, S. Brooker, *J. Am. Chem. Soc.* **2012**, *134*, 2892–2894.
[41] M. G. Cowan, S. Brooker, *Dalton Trans.* **2012**, *41*, 1465–1474.
[42] R. G. Miller, S. Narayanaswamy, S. M. Clark, P. Dera, G. B. Jameson, J. L. Tallon, S. Brooker, *Dalton Trans.* **2015**, *44*, 20843–20849.

Manuscript received: November 22, 2021
Accepted manuscript online: January 15, 2022
Version of record online: February 2, 2022